BEGINNING AND END OF ANNUAL RAIN SEASON IN THE NORTHWESTERN PART OF MADAGASCAR

MAXWELL Djaffard[1], DONA Victorien Bruno[1], RAKOTOVELO Geoslin[1], RATIARISON Adolphe Andriamanga[2]

[1]*Laboratory of Applied Physics and Renewable Energies, Mahajanga University, Madagascar*
[2]*Laboratory of Atmospheric, Climate and Ocean Dynamics, University of Antananarivo, Madagascar*

ABSTRACT

This article presents the study of the beginning and end of the rainy season in the northwestern part of Madagascar, delimited by latitudes -14 ° and -18 ° and longitudes 44 ° to 48 °. The study area experienced a significant upward trend in precipitation of 0.03 mm per year and an increase of 0.2 mm after the rupture date of 2006. This area can be subdivided into 4 regions in relation to precipitation.
Modeling and forecasting of the beginning and end of the area's rainy season was conducted. The results reveal that a sixth degree polynomial method is adapted to model the rainfall regime of the zone and subsequently simulate its future regime by the ARIMA method.

Keyword: *rainfall, climatological mean, anomaly, trend, Mann-Kendall test, Pettitt test, Principal Component Analysis, Anomalous Accumulation, sixth degree polynomial, ARIMA.*

1. INTRODUCTION

Rainfall is an important parameter in the study of climate change. The situation is such that in some countries the deluvian rainfall phenomenon becomes more frequent while others suffer from drought. This has an effect on the world economy, in particular in the agricultural and livestock sector.
Faced with this problem, what about Madagascar ? **Figure 1** shows the study area in the north-west of the large island. It is bounded by latitudes -14° and -18° and longitudes 44° to 48°, included in the blue rectangle.

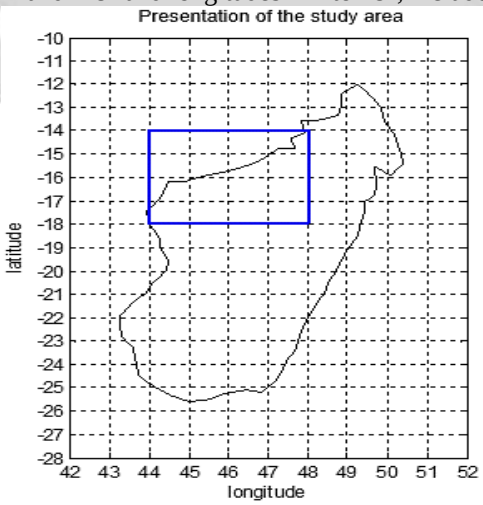

Figure 1: Representation of the study area

2. METHODOLOGIES

2.1 Data

These are daily precipitation reanalysis data, 1° x 1° spatial resolution over the period 1985 to 2015, from ECMWF

2.2 Methods

The methodology applied is to use:

- the Liebmann method "Anomalous Accumulation" which calculates the difference between the daily precipitation accumulation and the average theoretical accumulation during which it would precipitate daily (average daily rate). The beginning and the end of the rainy season are respectively defined by the abscissa date of the minimum and the abscissa date of the maximum of the curve. **[1] [2]**

$$AA(t) = \sum_{n=1}^{t} R(n) - \overline{R} * t \text{ with } \begin{cases} AA(t): \text{ Anomalous Accumlation} \\ \overline{\text{R}} \text{ daily mean of precipitation} \\ \text{R(n) : precipitation at day n} \end{cases}$$

- the sixth-degree polynomial method which filters data values according to a sixth-degree polynomial. After filtering, the curve has the equation of form : **[1]**

$$P(x) = p_6x^6 + p_5x^5 + p_4x^4 + p_3x^3 + p_2x^2 + p_1x + p_0$$

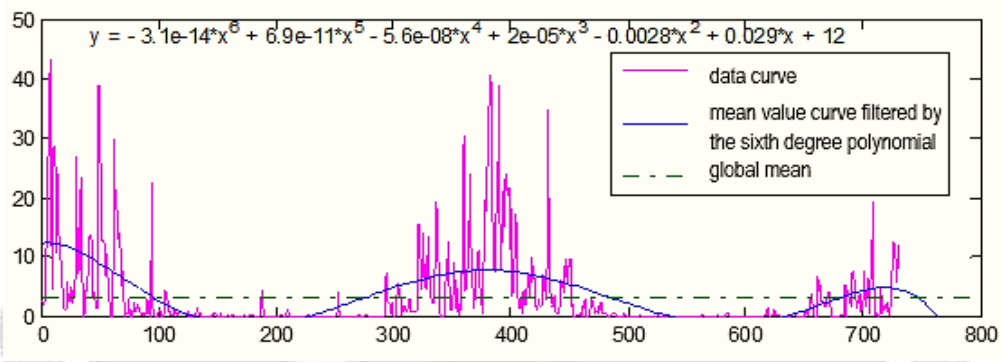

Figure 2 : typical presentation of the sixth degree polynomial method

- **Principal Component Analysis** (PCA), which is a factorial dimension reduction method for the statistical exploration of complex quantitative data. This method is widely used in the analysis of climatological data. **[3], [4], [5], [6]**

  - For two statistical series $k = (x_k, n_k)$ and $h = (x_h, n_h)$ of the same size n with a time depth of several years, the linear correlation coefficient is given by:

$$r(k,h) = \frac{1}{n}\sum_{i=1}^{n}\left(\frac{x_{ik} - \overline{x_k}}{s_k}\right)\left(\frac{x_{ih} - \overline{x_h}}{s_h}\right) \text{ with } \begin{cases} \overline{x_k}: \text{mean of k} \\ s_k: \text{standard deviation of k} \end{cases} \begin{cases} \overline{x_h}: \text{mean of h} \\ s_h: \text{standard deviation of h} \end{cases}$$

  - Data matrix:

Iinitial data table

$$T = \begin{pmatrix} v_{11} & v_{21} & \cdots & v_{1(p-1)} & v_{1p} \\ v_{21} & v_{22} & \cdots & v_{2(p-1)} & v_{2p} \\ \vdots & \vdots & \cdots & \vdots & \vdots \\ v_{(n-1)1} & v_{(n-1)2} & \cdots & v_{(n-1)(p-1)} & v_{(n-1)p} \\ v_{n1} & v_{n2} & \cdots & v_{n(p-1)} & v_{np} \end{pmatrix}$$

Cloud point center of gravity

$$G = \begin{pmatrix} x_{G1} = \dfrac{\sum_{i=1}^{n} v_{i1}}{n} \\ \vdots \\ x_{Gp} = \dfrac{\sum_{i=1}^{n} v_{ip}}{n} \end{pmatrix}$$

Choosing G as the origin leads to the reduced data center table

$$T_{cr} = \begin{pmatrix} \dfrac{v_{11} - x_{G11}}{s_1} & \dfrac{v_{21} - x_{G21}}{s_2} & \cdots & \dfrac{v_{1(p-1)} - x_{G1(p-1)}}{s_{(p-1)}} & \dfrac{v_{1p} - x_{G1p}}{s_p} \\ \dfrac{v_{21} - x_{G21}}{s_1} & \dfrac{v_{22} - x_{G22}}{s_2} & \cdots & \dfrac{v_{2(p-1)} - x_{G2(p-1)}}{s_{(p-1)}} & \dfrac{v_{2p} - x_{G2p}}{s_p} \\ \vdots & \vdots & \cdots & \vdots & \vdots \\ \dfrac{v_{(n-1)1} - x_{G(n-1)1}}{s_1} & \dfrac{v_{(n-1)2} - x_{G(n-1)2}}{s_2} & \cdots & \dfrac{v_{(n-1)(p-1)} - x_{G(n-1)(p-1)}}{s_{(p-1)}} & \dfrac{v_{(n-1)p} - x_{G(n-1)p}}{s_p} \\ \dfrac{v_{n1} - x_{Gn1}}{s_1} & \dfrac{v_{n2} - x_{Gn2}}{s_2} & \cdots & \dfrac{v_{n(p-1)} - x_{Gn(p-1)}}{s_{(p-1)}} & \dfrac{v_{np} - x_{Gnp}}{s_p} \end{pmatrix}$$

Reduced centered coordinates of the individual u_i:

$$X_{cri} = \begin{pmatrix} \dfrac{v_{i1} - x_{Gi1}}{s_1} \\ \vdots \\ \dfrac{v_{ip} - x_{Gip}}{s_p} \end{pmatrix}$$

Total inertia of the cloud of individuals :

$$I_G = \frac{1}{n}\sum_{i=1}^{n}\sum_{j=1}^{p}\left(\frac{v_{ij} - x_{Gij}}{s_j}\right)^2 = \sum_{j=1}^{p}\left(\frac{1}{n}\sum_{i=1}^{n}\left(\frac{v_{ij} - x_{Gij}}{s_j}\right)^2\right) = \sum_{j=1}^{p}\left(\mathrm{r}\left(v_{ij}\right)\right)$$

Covariance matrix:

$$R = \begin{pmatrix} r(v_{11}) & r(v_{12}) & \cdots & r(v_{1(p-1)}) & r(v_{1p}) \\ r(v_{21}) & r(v_{22}) & \cdots & r(v_{2(p-1)}) & r(v_{2p}) \\ \vdots & \vdots & \cdots & \vdots & \vdots \\ r(v_{(p-1)1}) & r(v_{(p-1)2}) & \cdots & r(v_{(p-1)(p-1)}) & r(v_{(p-1)p}) \\ r(v_{p1}) & r(v_{p2}) & \cdots & r(v_{p(p-1)}) & r(v_{pp}) \end{pmatrix} = \begin{pmatrix} 1 & \cdots & & & \\ \vdots & 1 & \cdots & & \\ \cdots & \cdots & 1 & \cdots & \\ & & \cdots & 1 & \cdots \\ & & & \cdots & 1 \end{pmatrix}$$

$$\text{so } trace(R) = p = I_G$$

- Eigenvalues and eigenvectors :

$$T_{cr}(V) = \lambda V \text{ where } \begin{cases} \lambda : \text{ eigenvalue} \\ \text{V: eigenvector} \end{cases}$$

Axes Δ_i passing through G and minimum inertia have for vector director eigenvectors V_i associated with eigenvaluess λ_i such as

$$I_G = \sum_{i=1}^{p} \lambda_i$$

- Selection of the principal axes to be chosen

$$\sum_{i=1}^{p} \lambda_i = p \Rightarrow \overline{\lambda} = \frac{\sum_{i=1}^{p} \lambda_i}{p} = 1 \text{ therefore we can not consider as significant that the } \lambda_i \geq 1$$

By Kaiser's empirical criterion, by centering and reducing the data, we retain the principal components corresponding to eigenvalues greater than 1. **[7]**

- Quality of representation of an individual u_i on an axis Δ_k

The parameter $cos^2\theta$ is used to characterize the quality of representation (qlt) on an axis**. [7], [8], [9]**

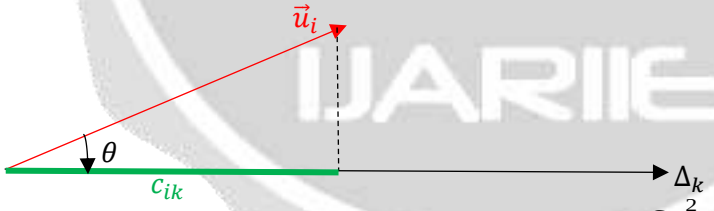

$$qlt_k(\vec{u}_i) = \cos^2(\theta) = \frac{c_{ik}^{\,2}}{\left\|\vec{u}_i\right\|^2}$$

$$\left\|\vec{u}_{ik}\right\|^2 = \sum_{k=1}^{p} c_{ik}^{\,2}$$

The closer qlt_i is to 1, the better it is represented.
The closer qlt_i is to 0, the more it is misrepresented.

Quality of representation of variables**. [3], [4], [5]**
On a factorial plane defined by two pricipal axes :

- a variable close to the correlation circle is well represented in this plane;
- a variable close to the origin of the correlation circle is poorly represented in this plane.

- **the autoregressive model - moving mean**

➢ **ARMA**(p, q) process **[10], [11]**

The autoregressive - moving mean (ARMA), is characterized by a p parameter of the autoregressive part and a q parameter of the moving mean part. An ARMA(p, q) process checks the equation:

$$X_t = \phi_1 Xt\text{-}1 + ... + \phi_p X_{t-p} + E_t + \theta_1 E_{t-1} + ... + \theta_q E_{t-q} \text{ in other words } \Phi(B)X_t = \Theta(B)E_t.$$

The treatment of a such process is complex. It can be shown, however, that its autocorrelations and partial autocorrelations are depreciated functions tending towards 0 in absolute value at exponential speeds.
Analysis of correlograms is one of the preferred tools in model identification.

➢ ARIMA(p, d, q) model

A process X_t admits a polynomial trend of degree d, the differentiated process d times is stationary:

$$Y_t = \Delta^d X_t = (I\text{-}B)^d X_t.$$

The ARIMA model comes down to applying an ARMA model on the differentiated process:

$$Y_t = \text{ARMA}(p, q) \Leftrightarrow X_t = \text{ARIMA}(p, d, q).$$

The equation of an ARIMA(p, d, q) model is therefore given by:

$$\Phi(B)Y_t = \Theta(B)E_t \Leftrightarrow \Phi(B)\Delta^d X_t = \Theta(B)E_t$$

where Φ and Θ are two polynomials of respective degrees p and q. The 'I' of ARIMA means 'integrates' as a reciprocal of differentiation.
Degree d is not generally known. To determine it we can act by trial and error or resort to stationarity tests: since an ARMA process (p, q) is stationary, we try to accept the hypothesis of stationarity for the process $Yt = \Delta^d X_t$. In general, we refer to a parsimony principle and look for the minimum satisfying value of d.

3. RESULTS AND DISCUSSIONS

3.1 Climatological mean of rainfall from 1985 to 2015 in the study area

Figure 3 shows the curves of daily and monthly climatological mean of precipitation in the study area. The red and green curves are the climatological mean of daily precipitation and the climatological mean of monthly precipitation over the study period, respectively.
The maximum daily climatological mean of precipitation is 19.89 mm (mean of precipitation on 28 January).
The maximum monthly climatological mean of precipitation is 12.26 mm (mean of precipitation of the months of February)

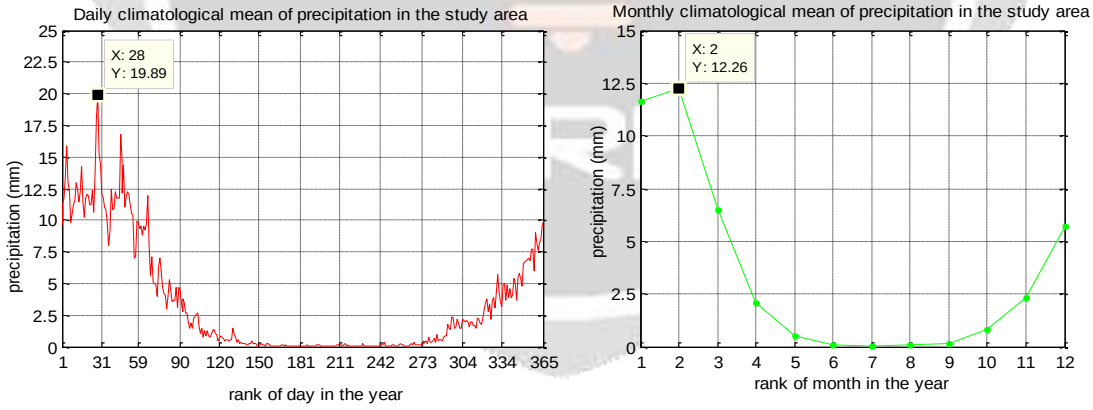

Figure 3 : Variation of the daily and monthly climatological mean of the precipitations

3.2 Evolution of annual mean rainfall since 1985 to 2015

Figure 4 shows the evolution of the annual mean precipitation in the study area. The purple line represents the trend of the evolution. It is of equation $y = 0,031x + 3,016$ where the origin is the year 1985. The slope being positive therefore the precipitation has an upward trend of 0.031mm per year. . Mann Kendall's test gives a p-value equal to 0.0228. As this value is well below 0.05, the trend is significant.

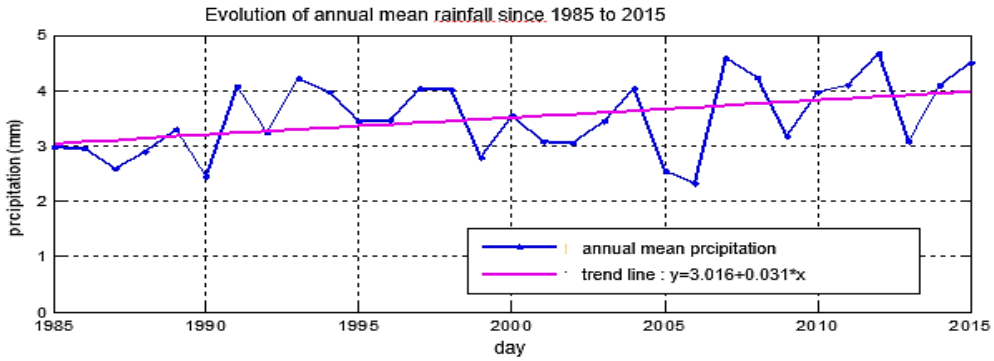

Figure 4 : annual mean precipitation curve and trend line

3.3 Annual precipitation anomaly from 1985 to 2015

The moving average curve of the annual anomaly is increasing from negative to positive. As a result, there were generally 2 distinct periods predominating in the time series: initially a relatively less rainy period from 1985 to 1999 and then an increasingly rainy period from 2001 to 2015. **(Figure 5)**

There was a precipitation deficit between 1985 and 1990. The series is then marked by a quasi-pseudoperiodic alternation of positive and negative anomalies between 1991 and 2006. From 2007 onwards there is a predominance of positive annual anomalies. The extremal values occurred in 2006 (negative anomaly -1.19 mm) and in 2012 (positive anomaly +1.15 mm).

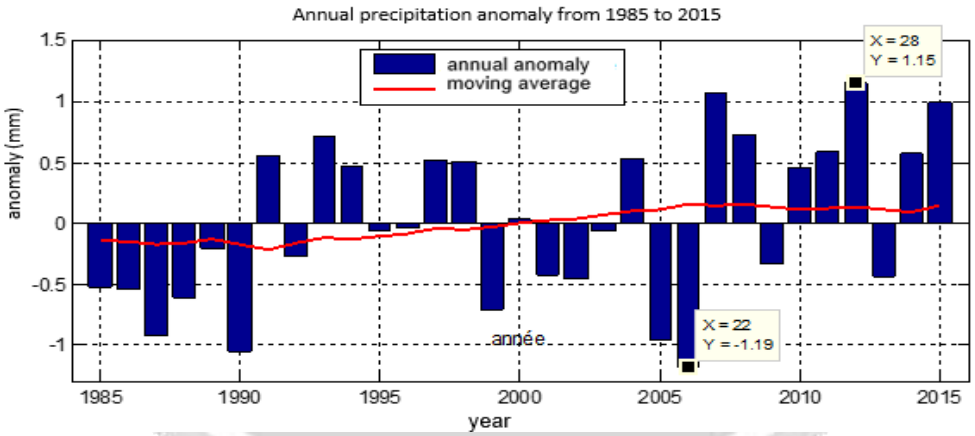

Figure 5 : Annual precipitation anomaly from 1985 to 2015

3.4 Observation of climate change relative to rainfall in the study area

Figure 6 shows the curves of the Pettitt test applied to precipitation over the 1985-2015 period. The curve reaches its maximum in 2006: it is the year of rupture.

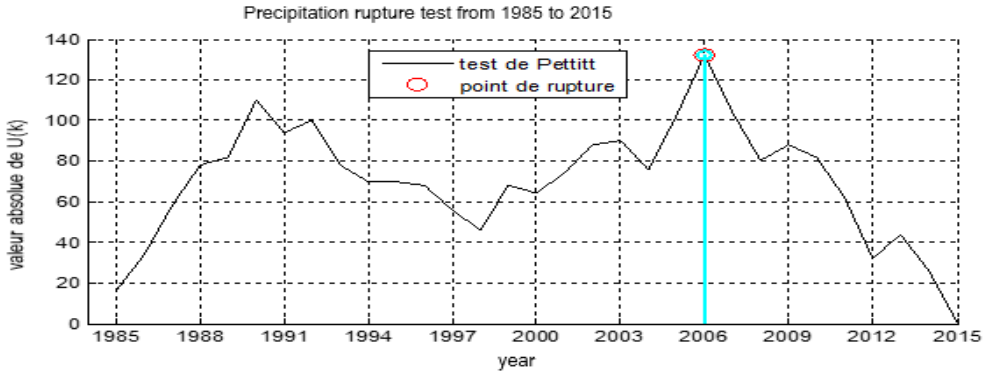

Figure 6 : Pettitt rupture test for precipitation

Table 1 gives the annual average of precipitation before and after the date of rupture. There is an overall increase in precipitation of about 0.2 mm in the study area after the rupture date.

Table 1: variation in mean precipitation

Climate variable	Average before date of rupture	Date of rupture	Average after date of rupture	Increase
precipitation	3.3010 mm	2006	3.5128 mm	0.211 mm

3.5 Principal Components Analysis results

In the principal component analysis study, all rainfall from each point of intersection of latitude and longitude in the study area at 1° x 1° spatial resolution was selected as individuals and variables were selected for the 12 months of the year. This gives 5 points according to latitude and 5 points according to longitude. As a result, there are 25 intersection points representing individuals. **(Figure 7)**

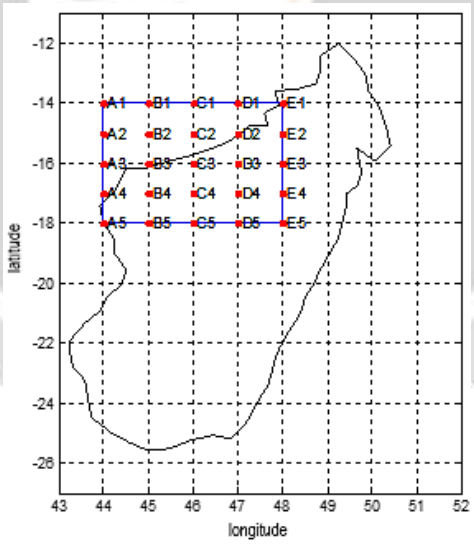

Figure 7 : representation of individuals in the study area

3.5.1 Choice of number of axis to be retained

Figure 8 shows the eigenvalue scree of the monthly mean precipitation. The Kaiser criterion allows to keep only the factorial axes F1 and F2 explaining 90.58% of the total inertia of the cloud to study the behaviour of each individual in relation to the others.

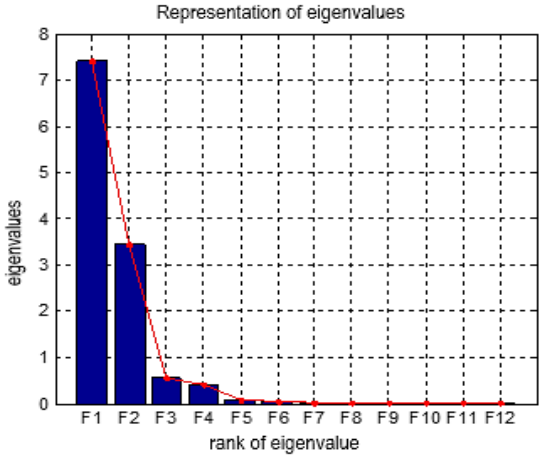

Figure 8 : representation of eigenvalues

3.5.2 Projections of variables on the factor plane F1-F2

Figure 9 shows the projection of the variables in the factor plane F1-F2. All variables are practically well represented in this factor plane.

The variables January, February, March, April, September, October, November and December are well correlated with the F1 axis. These months are mostly southern summer months. The most correlated month is March and the least correlated in this group is February. According to Figure 3, March has a lower monthly climatological mean of precipitation than February. As a first approximation, the F1 axis therefore orders the summer months in decreasing order of rainfall.

The variables May, June, July and August are well correlated with the F2 axis. The F2 axis therefore represents the southern winter months in the study area, characterized by very low monthly mean climatological rainfall as shown in **Figure 3**.

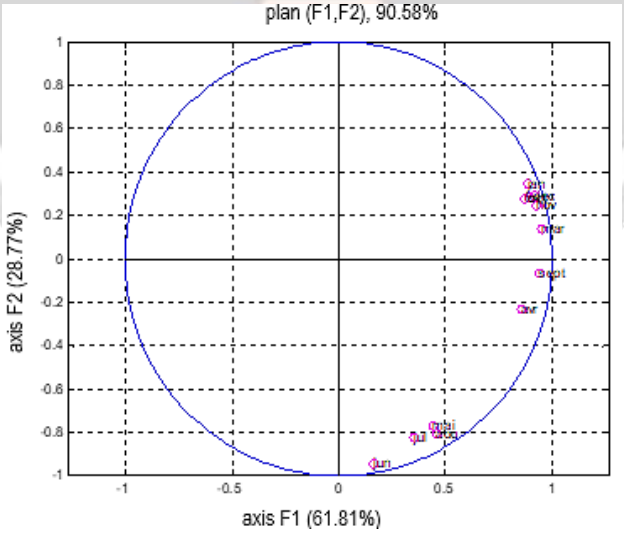

Figure 9 : projection of variables on the F1-F2 factorial plane

3.5.3 Projections of individuals on the F1-F2 factorial plane

Figure 10 shows the projection of individuals on the factorial plane F1-F2.

- The individual B4 makes the most F1 axis, so this individual is at relatively low rainfall during the southern summer as well as the individuals in his group.

- The individual E5 makes the most F2 axis, this individual receives almost no rain during the austral winter. It is the same for individuals in his group.
- Individual C5 is less coordinated than that of B4. As the F1 axis orders the summer months in decreasing order of rainfall, the group of individuals in the same category as C5 thus receives more rain than B4 during the southern summer.
- Individual C2 is virtually opposite to C5 on the F1 axis and positive coordinate on F2. This individual therefore receives more rain than the others in the summer and still receives some in the southern winter. Same for other individuals in his group.

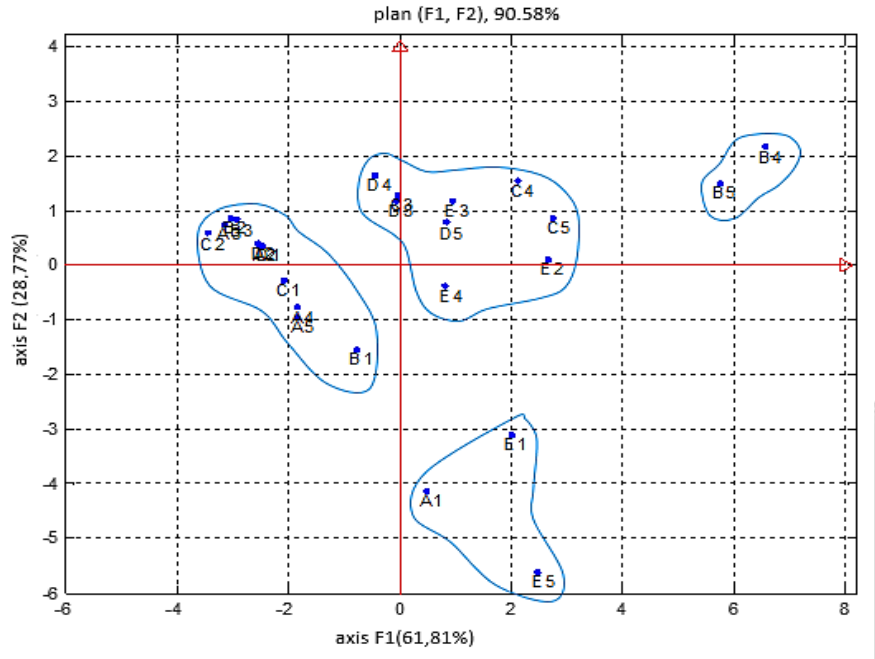

Figure 10 : projection of individuals on factor plane F1-F2 for precipitation

3.5.4 Regionalization of the study area

Taking into account the relationship between individuals and variables, the study area can be subdivided into 4 regions (**Figure 11**) :

region 1 : composed of **C3**, **C4**, **C5**, **D3**, **D4**, **D5**, **E2**, **E3** and **E4** (coloured blue). This region has relatively high rainfall in the southern summer.

region 2 : composed of **A2, A3, A4, A5, B1, B2, B3, C1, C2, D1** and **D2** (coloured red) **.** This region receives a large amount of rain in summer.

region 3 : composed of **A1**, **E1** and **E5** (coloured in yellow). It is a dry region in winter but with relatively high rainfall in southern summer.

region 4 : composed of **B4** and **B5** (coloured green) **.** It is a region that has a relatively low rainfall in summer.

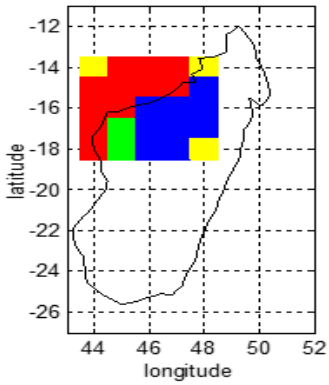

Figure 11 : distribution of regions with similar rainfall patterns

3.6 Forecast of beginning and end of rainy season in each region

Figure 12 shows the beginning of the rain season curves in the four regions. The curve in purple represents the real beginning and the curve in red the beginning foreseen by the method ARIMA.

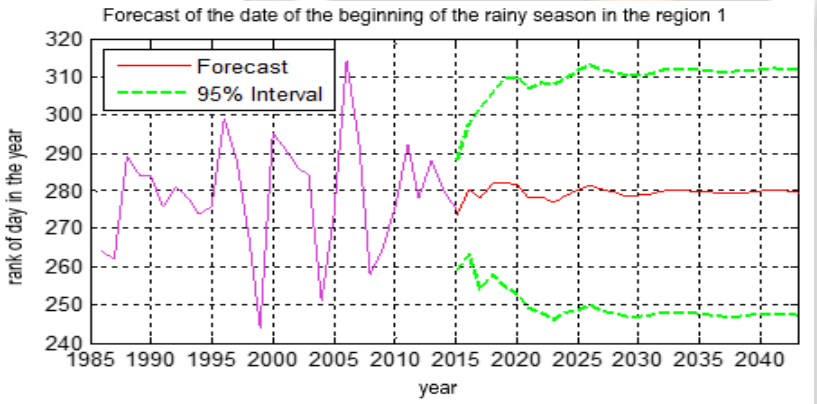

In Region 1, the forecast for the beginning of the rainy season would be around 280th day (October 7) from 2032 to 2043 At the origin of the start of the forecast in 2015, the expected start would have been 1.6 days ahead of the actual start.

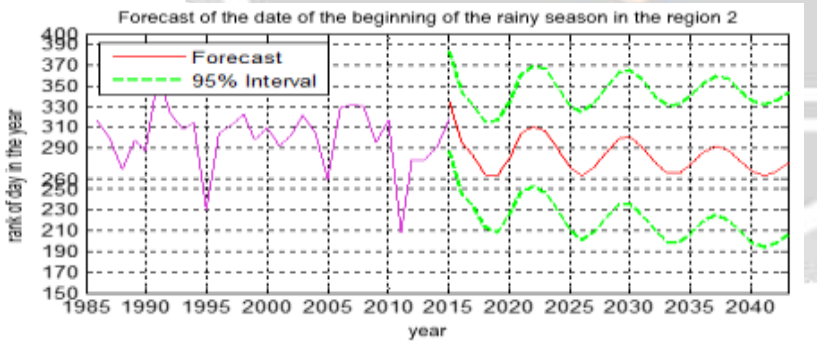

In Region 2, the forecast curve for the beginning of the rainy season would vary pseudoperiodically. Its maximum would gradually decrease. Its minimum would be practically constant, and would be around 260 days (17 September). At the origin of the start of the forecast in 2015, the expected start would have been 16.5 days behind the actual start.

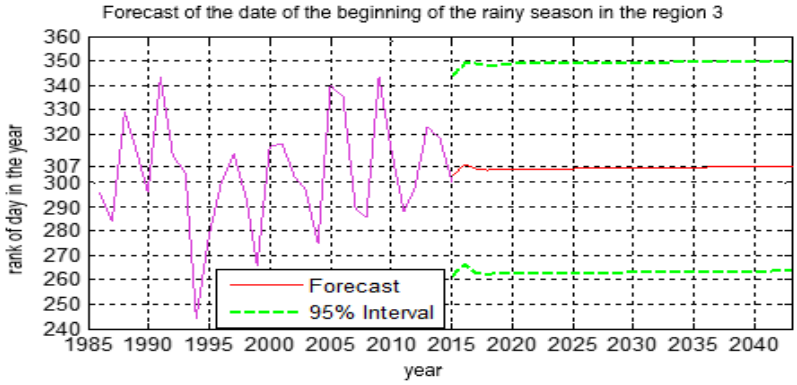

In Region 3, the forecast curve for the beginning of the rainy season would be virtually constant. The start date would be around 307th day (3 November) by 2043. At the origin of the start of the forecast in 2015, the expected start would have been 2.7 days behind the actual start.

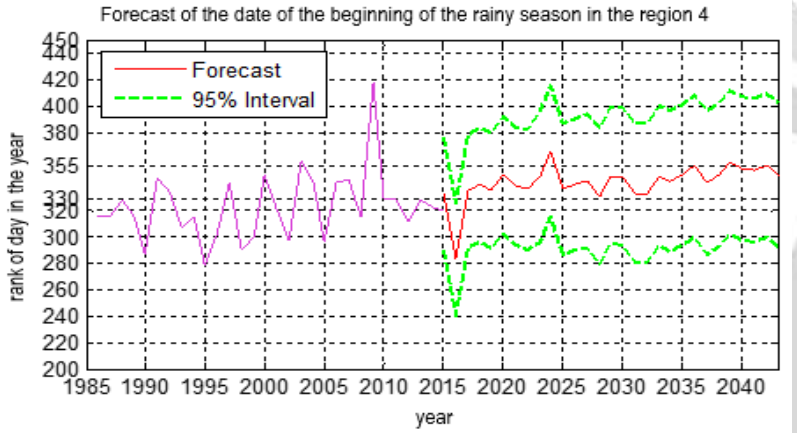

In Region 4, the forecast curve for the beginning of the rainy season would fluctuate between 330th and 355th days (between 26 November and 21 December) starting in 2025. At the origin of the start of the forecast in 2015, the expected start would have been 13.7 days behind the actual start.

Figure 12 : forecast of the beginning of the rain season in the 4 regions

Figure 13 shows the end of rainy season curves for the four regions. The blue curve represents the actual end and the red curve represents the end predicted by the ARIMA method.

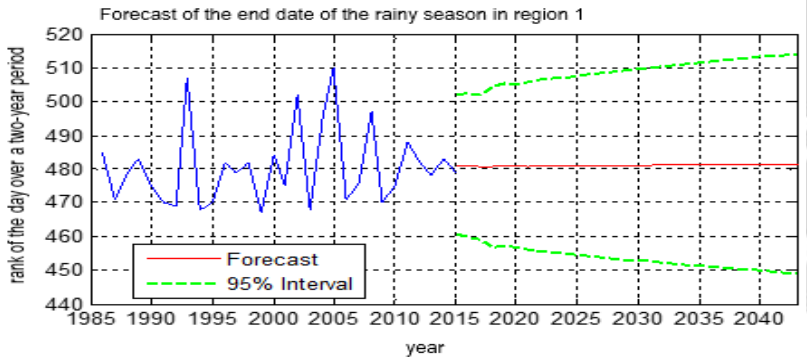

In Region 1, the forecast curve for the end of the rainy season would be almost constant and would remain around 480th day (April 25) until 2043. At the origin of the start of the forecast in 2015, the expected end would have been 2 days late compared to the actual end.

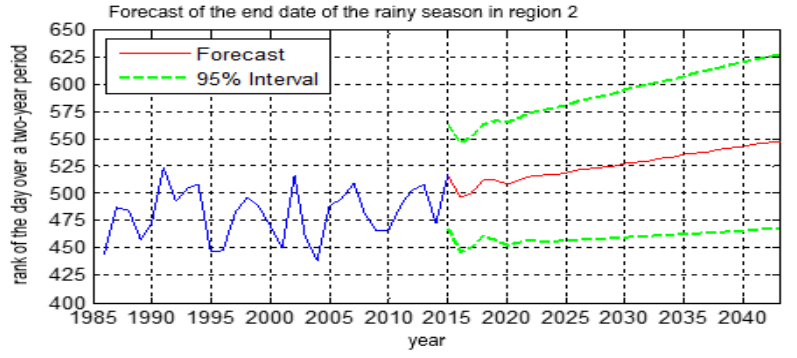

In Region 2, the forecast curve for the end of the rainy season would grow. As a result, the end of the rainy season would become more and more protracted. By 2043, the end of the rainy season would be around 550th day (4 July). At the origin of the start of the forecast in 2015, the expected end would have been 2.6 days ahead of the actual end.

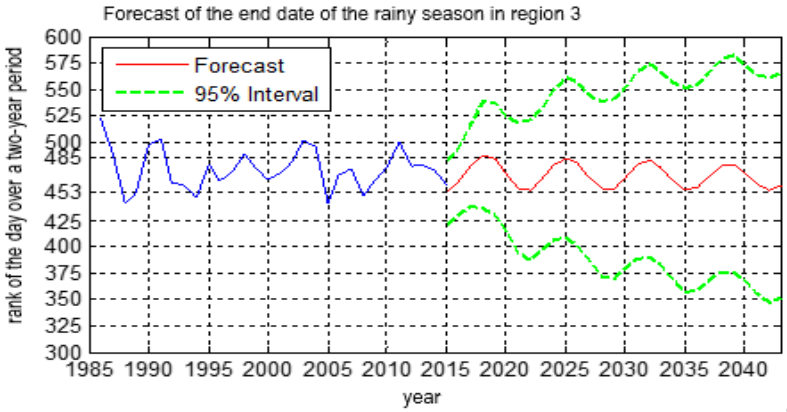

In Region 3, the forecast curve for the end of the rainy season would be almost sinusoidal. The end date would be between 453rd and 485th day (29 March and 30 April). At the origin of the start of the forecast in 2015, the expected end would have been 2.7 days ahead of the actual end.

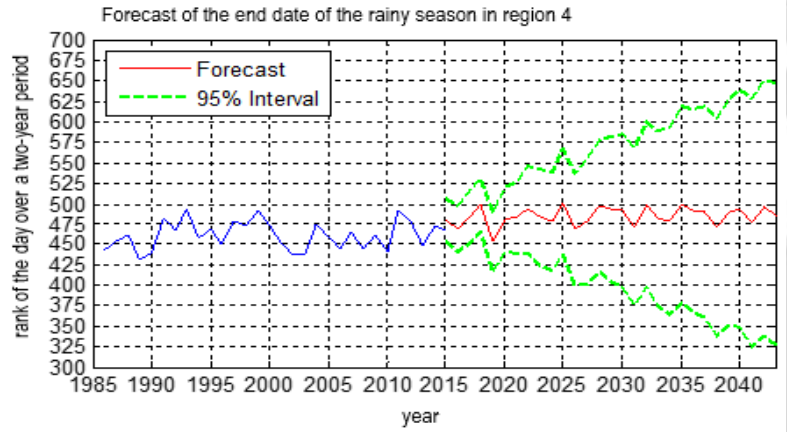

In Region 4, the end-of-season rain forecast curve would fluctuate between 475th and 500th day (between April 20 and May 15) from 2027. At the origin of the start of the forecast in 2015, the expected end would have been 12.3 days behind the actual end.

Figure 13 : forecast the end of the rainy season in the 4 regions

3.7 Modelling the beginning and end of the rainy season in the study area

- **Figure 14** shows the actual start curve, the start curve modelled by the Liebmann method (Anomalous Accumulation) and the start curve modelled by the sixth degree polynomial method of the rainy season in the study area. The trend line of the real start and the trend line of the beginning modelled by the sixth degree polynomial are positive slopes, unlike that modelled by the Liebmann method. The overall mean difference between the actual start and the start modelled by the **Liebmann method** is -26.33 days ; the difference between the actual start and the start modelled by the **sixth degree polynomial method** is 25.20 days. Taking into account the values of their slopes and their respective overall mean deviations, the result given by modelling by the sixth degree polynomial method is more precise than that given by the Liebmann method. The detection of the beginning of the rainy season by the sixth degree polynomial method is therefore more suitable in this study area than detection by the Liebmann method.

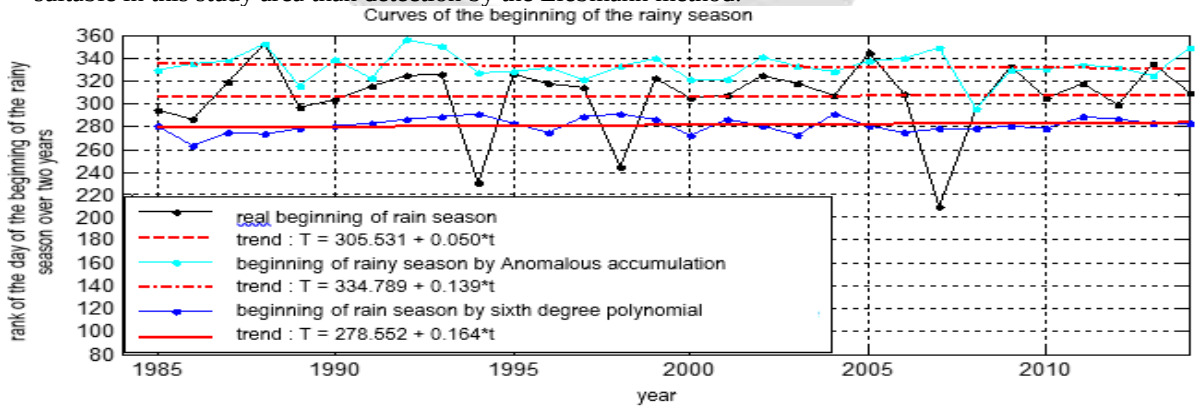

Figure 14 : curves of beginning of rainfall season in the study area

- **Figure 15** shows the real end curve, the end curve modelled by the Liebmann method (Anomalous Accumulation) and the end curve modelled by the sixth degree polynomial method of the rainy season in the study area. The real end trend line of the rainy season is on a positive slope. The end trend line modeled by the sixth degree polynomial and that modeled by the Liebmann method are negative slopes. The overall mean difference between the real end and the end modelled by the Liebmann method is 30.30 days; that between the real end and the end modelled by the sixth degree polynomial method is -21.43 days. The modelling of the end of the rainy season by these methods is less accurate than that of the beginning. However, on the basis of their respective slope values and overall mean deviations, modelling by the sixth degree polynomial method is more accurate than that by the Liebmann method, therefore more suitable in this study area.

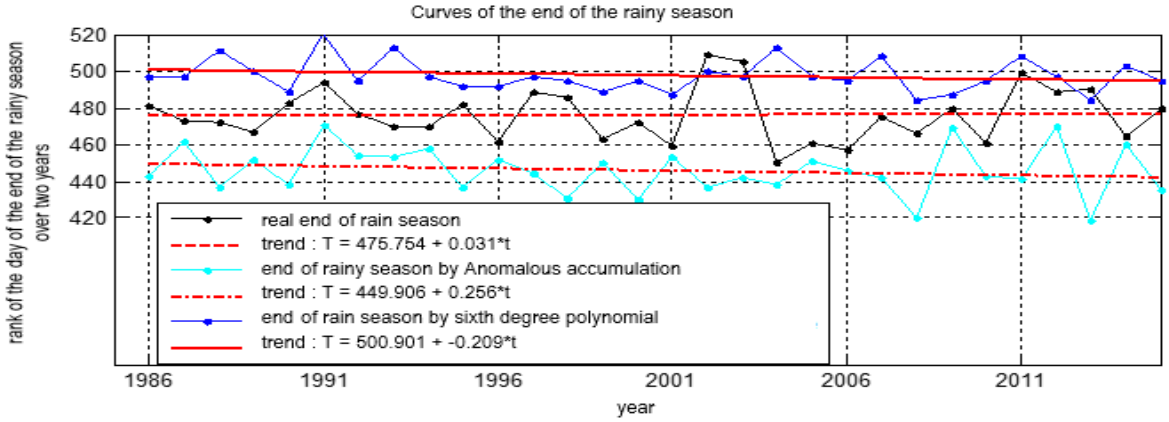

Figure 15 : curves of end of rainfall season in the study area

3.8 Forecast of the beginning and end of the rainy season in the study area

Figure 16 and **Figure 17**, respectively, represent predictions of the simulated start date, the simulated end date of the rainy season in the study area. Autocorrelograms (ACF), Partial Autocorrelograms (PACF), Residue Autocorrelograms (ACF) and Partial Residue Autocorrelograms (PACF) are also shown to verify the validity of the application of the forecast method used.

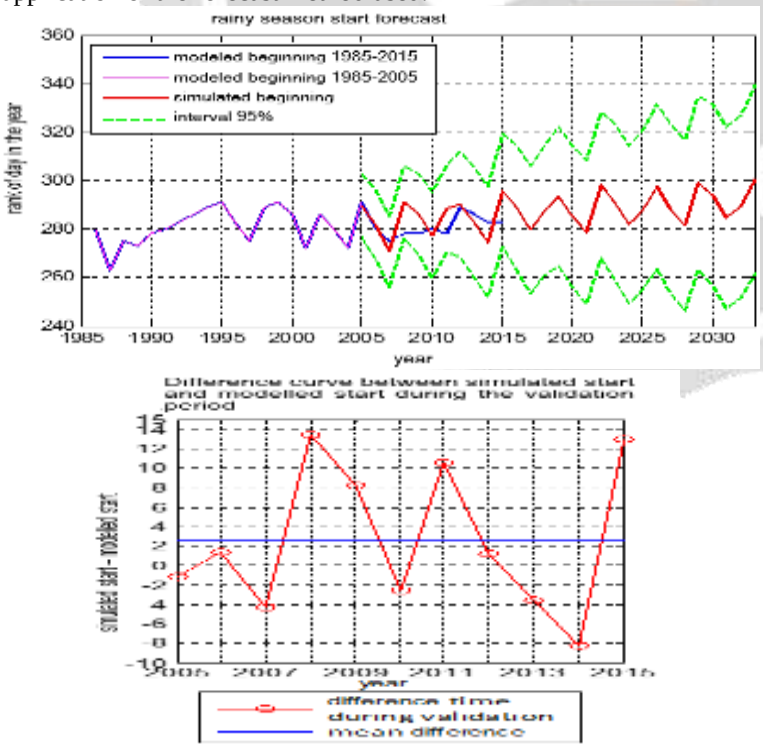

At the beginning of the 2005-2015 validation period, the simulated start is 1.1 days ahead of the modelled start.
During the validation period :
• the maximum lag is 13.38 days where the simulated start is behind the modelled start (in the fourth year of validation).
• average time difference is 2.53 days

At the end of the validation period, the simulated start is 13.01 days behind the modelled start.
The simulated start of the rainy season in the study area would be between 280th and 300th days (between 7 and 27 October).

Figure 16 : forecast of the end date of rainy season

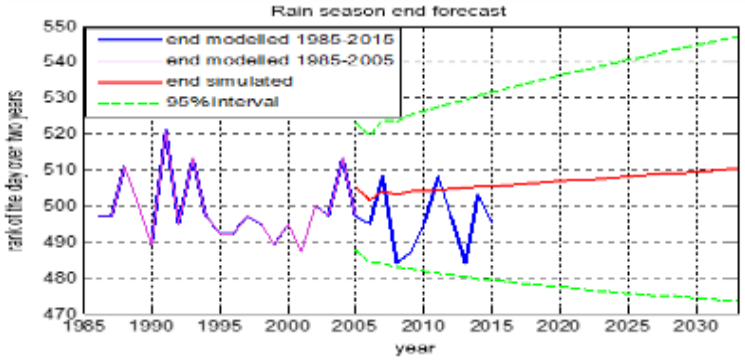

At the beginning of the 2005-2015 validation period, the simulated end is 8.34 days behind the modelled end.
During the validation period :
• the maximum offset is 20.89 days where the simulated start is behind the modelled start (in the 9th year of validation).
• average time difference is 8.51 days

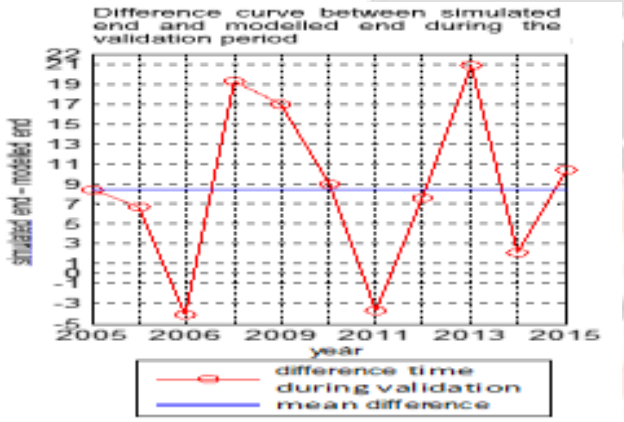

At the end of the validation period, the simulated end is 10.43 days late compared to the modelled end.
The simulated end of the rainy season in the study area would be around May 25 by 2033.

Figure 17 : forecast of the start date of rainy season

4. CONCLUSIONS

During the study period from 1985 to 2015, the northwestern part of Madagascar experienced a relatively less rainy period from 1985 to 1999 and an increasingly rainy period from 2001 to 2015. The annual mean precipitation trend was a significant increase of 0.03 mm per year. The year 2006 was the year of rupture marked by a 0.2 mm increase in the overall annual mean precipitation.

The study area can be subdivided into four regions with the same rainfall pattern:
- Region 1 has relatively high rainfall in southern summer;
- Region 2 receives a large amount of rain in southern summer;
- Region 3 is a dry region in the southern winter but with relatively high rainfall in the southern summer;
- Region 4 is a region with relatively low rainfall during the southern summer.

Forecasting the start and end date of the rainy season shows that:
- in Region 1, the beginning of the rainy season would be around 7 October from 2032 until 2043 and the end would be almost constant remaining around 25 April until 2043.
- in Region 2, the beginning would vary pseudoperiodically with a maximum that would gradually decrease. Its minimum would be practically constant, being near 17 September. The end will linger more and more. In 2043, it would be around July 4th.
- in Region 3, the beginning would be practically constant and would be around 3 November by 2043. The end would be between 29 March and 30 April.
- in Region 4, the beginning would fluctuate between November 26 and December 21 from 2025 and the end would fluctuate between April 20 and May 15 from 2027.

To simulate the season of the beginning and end of the rainy season in this study area, the sixth degree polynomial method is best suited for modelling. Predicting the beginning and end of the upcoming rain season using simulation by combining the model with the ARIMA method yielded:
- the simulated beginning of the rainy season in the study area would oscillate between 7 and 27 October;

- the simulated end of the rainy season in the study area would be increasingly lingering and would be around May 25 by 2033.

5. REFERENCES

[1] RAMIHARIJAFY Rodolphe : INTER-CORRELATION ENTRE LA PLUVIOMETRIE ET LE DEBIT SAUVAGE EN AMONT DE LA CENTRALE HYDROELECTRIQUE DU SITE D'ANDEKALEKA A MADAGASCAR. Thèse de doctorat, Université d'Antananarivo. Pages 76-78 ; 83-84

[2] RAZANATOMPOHARIMANGA Niry Havana : PREVISION DES PERIODES DE PLUIES (DEBUTS ET FIN) DANS LA PARTIE CENTRE-OUEST DE MADAGASCAR. Thèse de doctorat, Université d'Antananarivo 15/01/2016. Page 30-31

[3] N. Croiset, B. Lopez (BRGM), Outil d'analyse statistique des séries temporelles d'évolution de la qualité des eaux souterraines, Manuel d'utilisation, Rapport final, pp.18-19

[4] P. Besse www.math. univ-toulouse.fr/besse, M2 MASS, TP4 : Introduction au logiciel SAS Procédures statistiques multivariées : Analyse en Composantes Principales. Pages 1, 2.

[5] C.DUBY, S ROBIN ; Analyse composantes principale, juillet 2006. Pages 4,5.

[6] Aimé KOUDOU et al, CONTRIBUTION DE L'ANALYSE EN COMPOSANTES PRINCIPALES A LA REGIONALISATION DES PLUIES DU BASSIN VERSANT DU N'ZI, CENTRE DE LA COTE D'IVOIRE, 2015. Page 162.

[7] Ali Kouani, S. El Jamali et M.Talbi, Analyse en Composantes principales, Une méthode factorielle pour traiter les données didactique, février 2007. Page 3.

[8] ADD3-MAB, D-interpretation d'une ACP, 2011.Papes 4, 29.

[9] Jean-Marc Labatte, jean-marc.Labatte@univ-angers.fr, Analyse des données M2, consulté le 17 Février 2017.

[10] www.agroparistech.fr/IMG/pdf/Polychro.pdf, consulté le 5 Septembre 2018

[11] lacote.ensae.net/SE206/Cours/Joachim.Connault.pdf